*Iranian Journal of Materials Science and Engineering, Vol. 20, Number 4, December 2023*
RESEARCH PAPER

# Unveiling the Effect of Annealing Temperature on the Phase Transformations of Inconel 718 Super alloy Manufactured by Additive Manufacturing

**Sajad Ghaemifar, Hamed Mirzadeh***

* *hmirzadeh@ut.ac.ir*

School of Metallurgy and Materials Engineering, College of Engineering, University of Tehran, Tehran, Iran

**Received: July 2023** **Revised: December 2023** **Accepted: December 2023**
***DOI: 10.22068/ijmse.3304***

**Abstract:** *Phase transformations and the evolution of hardness during elevated-temperature annealing of Inconel 718 superalloy manufactured by the laser powder bed fusion (L-PBF) were investigated. The microstructural evolution, elemental analysis, phase formation, and hardening were characterized by scanning electron microscopy, energy-dispersive spectroscopy, X-ray diffraction, and Vickers indentation test, respectively. It was observed that the effect of annealing treatments is directly governed by the annealing parameters (i.e. time and temperature), for which the hardness measurement as a fruitful and convenient tool can reveal this effect. The increase of the hardness, which was obtained by the annealing (aging) treatments at the temperature range of 800-900°C, indicated precipitation of the $Ni_3Nb$ γ″ strengthening phase; while owing to the coarsening of precipitates as a result of overaging at this temperature range, the hardness decreased. For instance, the length and aspect ratio of precipitates in the aged sample at 800°C for 1 h are 67.14 nm and 0.32, respectively; while these values in the aged sample at 800°C for 8 h are 78.34 nm and 0.44, respectively. On the other hand, the decrease of the hardness at temperatures of 950 and 1000°C was attributed to the decrease of dislocation density in conjunction with the $Ni_2Nb$ Laves phase dissolution. Hence, it is crucial to determine the annealing parameters according to the required microstructure and properties.*

***Keywords:*** *Nickel-based superalloys, Additive manufacturing, Aging heat treatment, Homogenization treatment, Precipitation strengthening.*

## 1. INTRODUCTION

Ni-based superalloys are well-known engineering materials, which are widely used in various industries such as petroleum, energy generation, and aerospace [1, 2]. The Inconel 718 (IN718) superalloy is one of the most utilized alloys in this category, which is known as an age-hardening superalloy with favorable weldability [3-5].

Owing to the good weldability of IN718, the additive manufacturing (AM) process is a convenient method for the fabrication of IN718 parts with complex geometry [6, 7]. Laser powder bed fusion (L-PBF) is one of the most important AM methods for manufacturing metallic parts [8-13]. Recently, the fabrication of IN718 parts using the L-PBF method has been reported in many studies [14, 15]. Furthermore, performing the post-heat treatment is crucial to obtain favorable properties in the AM parts [16, 17].

Various annealing treatments as the post-processing of the IN718 manufactured by the L-PBF method have been reported in recent studies, including homogenization [18, 19] and aging treatment [20, 21]. It has been reported that these heat treatments might result in the potential phase transformation such as Laves phase dissolution as well as the precipitation of γ′, γ″, and δ phases, which also depends on the temperature and time of the heat treatment process. The main strengthening phases are γ′and γ″ phases; while the growth of the δ phase occurs at the expense of γ" phase, leading to the deterioration of the precipitation hardening effect, and generally impairing the creep resistance [22, 23]. Moreover, the importance of the time and temperature and their effect on the kinetics of the phase transformation has been studied in recent studies on the IN718 fabricated by cast [24], wrought [25], and L-PBF [18] processes. For instance, the activation energy for the dissolution of Laves phase in a cast sample was determined by the JMAK model as ~274.5 kJ/mol [24]; while this activation energy in an L-PBF sample was determined as ~160 kJ/mole [18], which shows the effect of the manufacturing process. Furthermore, it has been reported that utilizing hardness measurements is a useful tool to trace the evolution of phase transformations [26, 27].

Although many investigations have been performed on annealing at a specific temperature range, the effect of annealing at a wide


[ DOI: 10.22068/ijmse.3304 ]

temperature range to reveal its effect on the phase transformation and hardness values are not scrutinized yet and needs systematic investigation. Hence, the current study is dedicated to achieving these aims by determining the annealing parameters according to desirable microstructure and properties.

## 2. EXPERIMENTAL PROCEDURES

The L-PBF process was performed by using IN718 powder (EOS NickelAlloy IN718, EOS Company, Germany) with particle diameters in the range of 15-50 µm (Fig. 1a) and with adopting a commercial LPBF machine (SLM machine, ST). The process was performed by the above machine, equipped with a 100 W Nd-YAG laser, with a laser spot diameter of 50 µm. The protective atmosphere was argon, and the oxygen content inside the chamber was kept below 0.2%. Moreover, the process parameters are as follows: laser power of 95 W, scanning speed of 800 mm/s, hatching distance of 0.05 mm, layer thickness of 0.025 mm, and scanning strategy of stripe/67°. The annealing treatment was performed at the temperature range of 800-1000°C for a duration of 0.5 to 8 h. The samples were etched with the waterless Kaling's 2 reagents. Afterwards, a field-emission scanning electron microscope (MIRA3 TESCAN FESEM) was utilized for microstructural analysis. Image analysis was performed by the ImageJ software version 1.54 on the FESEM images. The Vickers indentation test (Wilson Tukon 1202 hardness tester) was utilized for the hardness measurements with a load of 5 kg, for which at least five indentations were averaged. It is noteworthy to state that for each heat treatment condition, 3 samples were prepared and the hardness testing was performed on them to check the reproducibility of the results and avoid any potential bias. X-ray diffraction (using a PHILIPS diffractometer with Cu-ka radiation) was performed for phase identification using the scan rate of 2°/min.

## 3. RESULTS AND DISCUSSION

### 3.1. As-built Microstructure

The FESEM image of the as-built sample is shown in Fig. 1b. It can be seen that the microsegregation (occurring during solidification [28, 29]) resulted in the formation of Laves phase (bright regions labelled as S2), which is consistent with the previous studies [16-18]. In other words, the microstructure of the as-built sample consists of the austenite phase (dark regions labelled as S1) and the mentioned phase. Furthermore, adopting the EDS analyses, Table 1 shows that the leaves phase is in the form of $Ni_2Nb$ due to the atomic ratio of Ni/Nb ~1.99. The aforesaid form of the Laves phase has been reported in previous studies [30, 31].

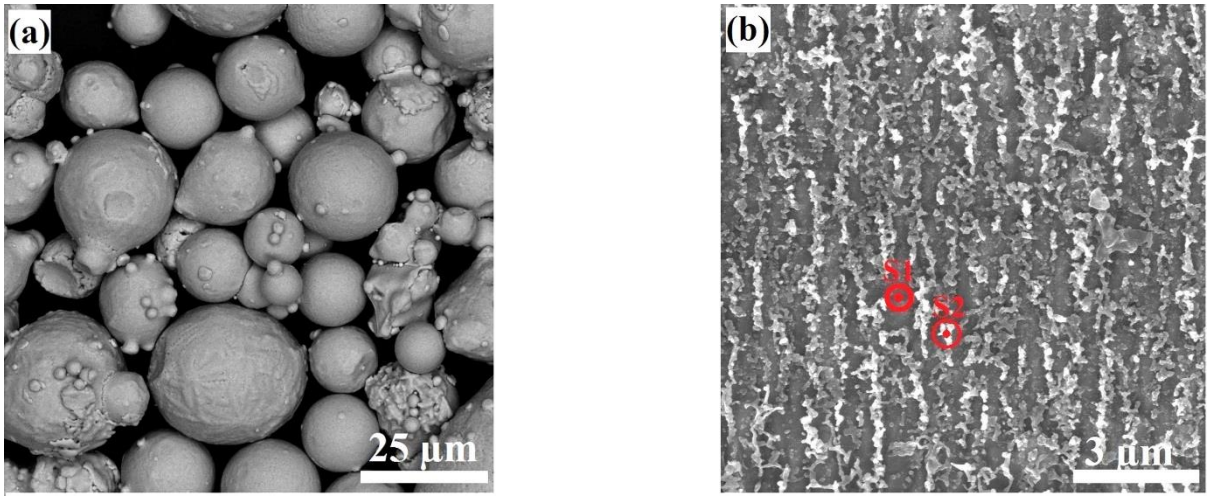


**Fig. 1.** (a) Atomized powder particles and (b) microstructure of the as-built sample.

**Table 1.** EDS results representing the elemental analysis (at %) of spots shown in Fig. 1

| Analyzed Spot | Ni | Cr | Nb | Mo | Ti | Al | Fe |
|---|---|---|---|---|---|---|---|
| Spot 1 (Austenite matrix) | 54.02 | 20.95 | 2.98 | 2.37 | 1.03 | 0.63 | 18.02 |
| Spot 2 (Laves phase) | 32.94 | 23.45 | 16.54 | 1.04 | 1.26 | 8.98 | 15.79 |





[ DOI: 10.22068/ijmse.3304 ]

### 3.2. Evolutions of the Hardness and Microstructure during Annealing

Fig. 2 shows the evolution of the hardness during annealing treatment at 800-1000°C. The results are also summarized in Table 2, for which the assigned name to the sample follows the pattern of Ax-y, where x and y represent the annealing temperature (°C) and time (h), respectively. Vividly, the variation of hardness values during annealing is directly related to the annealing temperature: At the temperature range of 800-900°C, the hardness increased during annealing; while at the temperatures of 950 and 1000°C, the reverse behavior can be seen. Therefore, two approximate temperature ranges of T< 950°C and T ≥950°C can be considered, as will be discussed in the following sections.

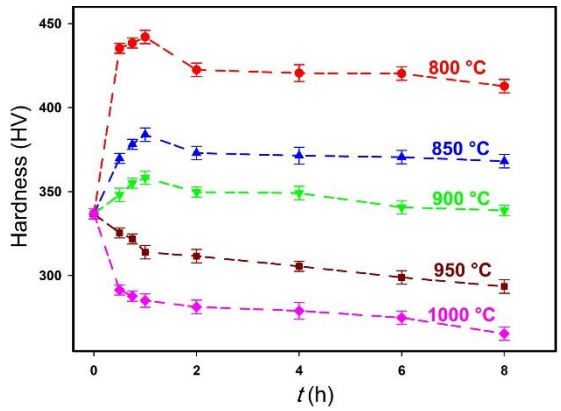


**Fig. 2.** Evolution of hardness during annealing at different temperatures.

### 3.3. Microstructural Evolution during Annealing at T< 950°C

As mentioned above, annealing at this temperature range leads to a significant increment of hardness, especially at the lower temperature of 800°C. Moreover, after reaching the peak hardness value, it decreases at long holding times. To find the reason behind these observations, a microstructural analysis should be performed. The microstructure of the A800-1 and A800-8 samples are shown in Fig. 3. It can be seen that along with the Laves phase with decreasing amount, new disk-shaped precipitates can be seen. Conducting EDS analysis on the observed disk-shaped precipitates shows that the atomic ratio of Ni/Nb in this phase is ~3.16 (Table 3), which is comparable to the ratio of 3 based on the stoichiometry of the γ″ phase ($Ni_3Nb$). It should be noted that the mentioned phase is reported in previous studies as the main precipitating phase during the aging of the IN718 superalloy processed by conventional methods [25, 32]. As shown in Fig. 4, the XRD pattern of the A800-1 sample confirms the precipitation of γ″ phase. Since the aging process is directly performed on the as-built sample, the Laves phase remained in the microstructure as confirmed by EDS analysis (Table 3). It has been stated that conducting aging treatment in the range of 650-900°C results in the precipitation of strengthening phases which leads to an increase in hardness [26, 33, 34]. Hence, the formation of these precipitates led to higher hardness values (for the annealing in the temperature range of 800-900°C) in comparison with the as-built sample. It can also be seen that the incremental behavior of the hardness values is sharply obtained at the first hour of aging treatment by reaching the peak hardness; while a longer aging time resulted in a decrease in hardness due to the occurrence of overaging, which is the consequence of the precipitate coarsening.

**Table 2.** Hardness values and the assigned names of different samples.

| Sample Name | Hardness (HV) | Sample Name | Hardness (HV) | Sample Name | Hardness (HV) | Sample Name | Hardness (HV) | Sample Name | Hardness (HV) |
|---|---|---|---|---|---|---|---|---|---|
| A800-0.5 | 435.2 ± 2 | A850-0.5 | 369.7 ± 2 | A900-0.5 | 348 ± 3 | A950-0.5 | 325.3 ± 2 | A1000-0.5 | 291.3 ± 2 |
| A800-0.75 | 438.5 ± 2 | A850-0.75 | 378.1 ± 2 | A900-0.75 | 355 ± 2 | A950-0.75 | 321.7 ± 2 | A1000-0.75 | 287.6 ± 2 |
| A800-1 | 442.1 ± 3 | A850-1 | 383.8 ± 2 | A900-1 | 358.2 ± 3 | A950-1 | 313.8 ± 2 | A1000-1 | 285.1 ± 3 |
| A800-2 | 422.4 ± 3 | A850-2 | 372.9 ± 3 | A900-2 | 349.6 ± 2 | A950-2 | 311.5 ± 3 | A1000-2 | 281.2 ± 3 |
| A800-4 | 420.5 ± 4 | A850-4 | 371.4 ± 4 | A900-4 | 349.1 ± 3 | A950-4 | 305.4 ± 3 | A1000-4 | 278.9 ± 4 |
| A800-6 | 420.3 ± 3 | A850-6 | 370.5 ± 3 | A900-6 | 340.5 ± 3 | A950-6 | 298.8 ± 4 | A1000-6 | 274.8 ± 3 |
| A800-8 | 412.7 ± 3 | A850-8 | 368.1 ± 3 | A900-8 | 338.7 ± 2 | A950-8 | 293.4 ± 3 | A1000-8 | 265.3 ± 3 |



[ DOI: 10.22068/ijmse.3304 ]

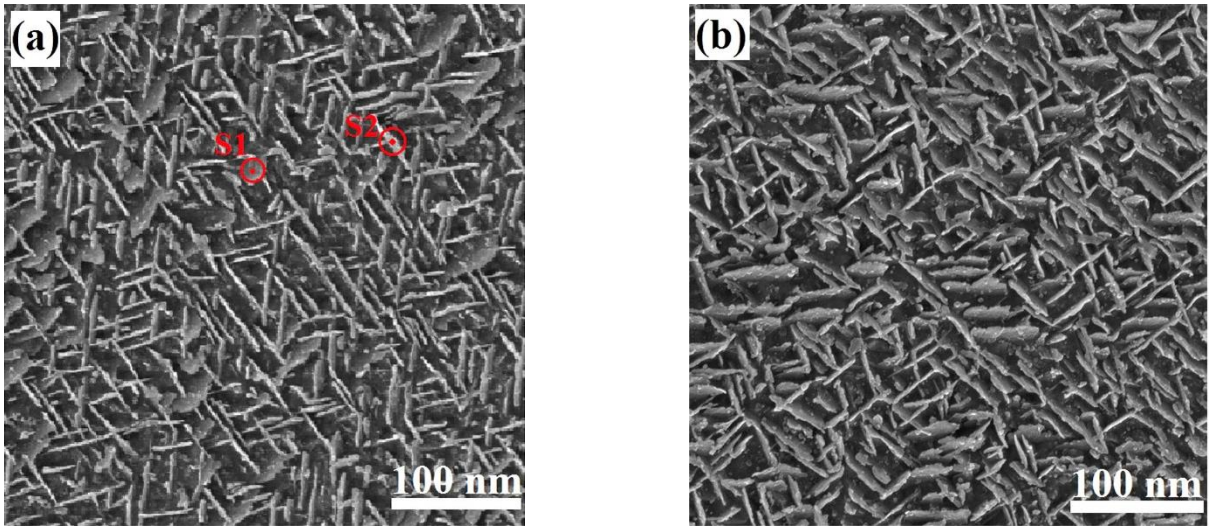


**Fig. 3.** Microstructure of the a) A800-1 and b) A800-8 samples.

**Table 3.** EDS results representing the elemental analysis (at %) of spots shown in Fig. 3

| Analyzed Spot | Ni | Cr | Nb | Mo | Ti | Al | Fe |
|---|---|---|---|---|---|---|---|
| Spot 1 (Laves phase) | 32.12 | 23.56 | 16.33 | 1.13 | 1.32 | 9.11 | 16.43 |
| Spot 2 (gamma double prime) | 36.08 | 22.86 | 11.42 | 1.64 | 1.41 | 10.06 | 16.53 |

In other words, the length and aspect ratio of precipitates in the A800-1 sample (peak aged sample, Fig. 3a) is 67.14 nm and 0.32, respectively; while these values in the A800-8 sample (overaged sample, Fig. 3b) is 78.34 nm and 0.44, respectively.

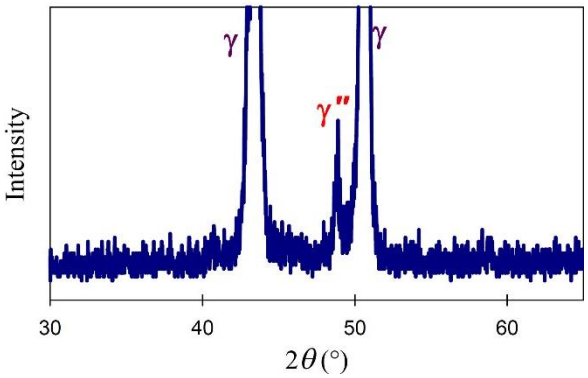


**Fig. 4.** XRD patterns of the A800-1 sample.

### 3.4. Microstructural Evolution during Annealing at T ≥950°C

As shown in Fig. 2, annealing at the temperatures of 950 and 1000°C led to a decrease in the hardness values, which implies that precipitation of the strengthening phases has not occurred. Moreover, it has been reported that performing annealing at the temperature range of 950-1250°C leads to the dissolution of the Laves phase [35, 36].

Fig. 5 shows the microstructure of the A1000-1 sample. It can be seen that the Laves phase is completely dissolved and a new phase has been precipitated.

The EDS analysis of this precipitate is shown in Table 4, which reveals the presence of a high amount of C and Nb atoms in this phase. Therefore, it can be inferred that the precipitated phase is the niobium carbide (NbC).

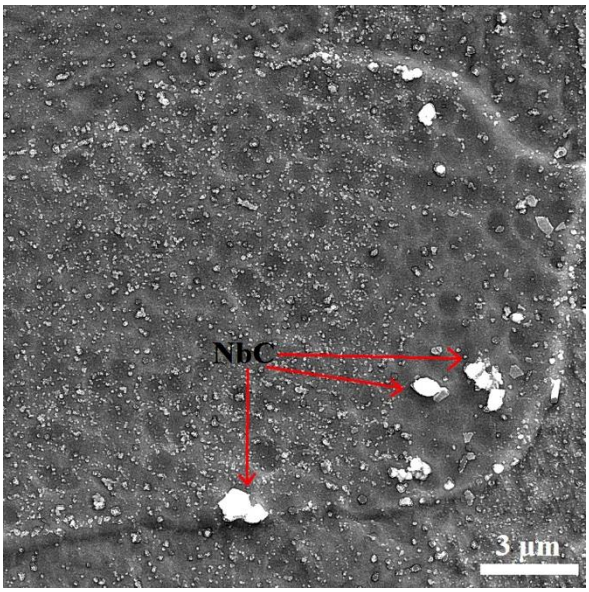


**Fig. 5.** Microstructure of the A1000-1 sample.



[ DOI: 10.22068/ijmse.3304 ]

**Table 4.** EDS results representing the elemental analysis (at %) of niobium carbide (NbC)

| Analyzed Spot | Ni | Cr | Nb | Mo | Ti | Al | Fe | C |
|---|---|---|---|---|---|---|---|---|
| Niobium carbide (NBC) | 17.91 | 1.89 | 22.13 | 0.61 | 5.03 | 1.28 | 1.28 | 49.87 |

The precipitation of the NbC during homogenization heat treatments in additively manufactured IN718 superalloy has been reported previously, while it is noteworthy to state that the volume fraction of the precipitated NbC (~0.4 %) is much less than values that can affect the hardness values [15, 37]. Moreover, it has been reported that the homogenization heat treatment, as a post-processing treatment, leads to a decrease in the initial dislocation density, which exists in the as-built sample owing to the fast solidification during the AM process [38-40]. Hence, it can be concluded that the decrease in the dislocation density along with the dissolution of the Laves phase resulted in the decrement in hardness values during annealing at temperatures of 950 and 1000°C.

In conclusion, it can be stated that the effect of annealing treatments is directly governed by the annealing parameters (i.e. time and temperature), for which the hardness measurement as a fruitful and convenient tool can reveal this effect. In other words, the increase of the hardness, which was obtained by the annealing (aging) treatments at the temperature range of 800-900°C, indicates precipitation of strengthening phases; while the decrease of the hardness is attributed to the decrease of dislocation density in conjunction with the Laves phase dissolution. Hence, it is crucial to determine the annealing parameters according to the required microstructure and properties.

## 4. CONCLUSIONS

The effects of annealing temperature on the phase transformation of Inconel 718 superalloy manufactured by additive manufacturing were investigated. The following conclusions can be drawn:

1) The microstructure of the as-built sample was composed of Laves phase in the austenite matrix. The stoichiometry of the Laves phase was in the form of $Ni_2Nb$ due to the atomic ratio of Ni/Nb ~1.99.
2) The effect of annealing treatments is directly governed by the annealing temperature and time, for which the hardness measurement as a fruitful and convenient tool can reveal this effect. Two approximate temperature ranges of T< 950°C (associated with the increment of hardness) and T ≥950°C (associated with the decrement of hardness) were considered.
3) The increase of the hardness, which was obtained by the annealing (aging) treatments at the temperature range of 800-900°C, indicated precipitation of the $Ni_3Nb$ $\gamma''$ strengthening phase. Moreover, after reaching the peak aged condition, overaging led to a decrement in hardness. In other words, as the annealing time increased, the size of the strengthening precipitates increased.
4) The decrease of the hardness at temperatures of 950 and 1000°C was attributed to the decrease of dislocation density in conjunction with the Laves phase dissolution.

## REFERENCES

[1]. Ghasemian Safaei, M., Rastegari, S. and Latifi, R., "The Effect of Powder Composition on Cyclic Oxidation Behavior of CO-Deposited Al-Si Cating on Nickle-Based Superalloy." Iran. J. Mater. Sci. Eng., 2020, 17, 92-103.

[2]. Lin, Y.C., Yang, H., He, D.G. and Chen, J., "A physically-based model considering dislocation–solute atom dynamic interactions for a nickel-based superalloy at intermediate temperatures." Mater. Des., 2019, 183, 108122.

[3]. Azarbarmas, M., Aghaie-Khafri, M., Cabrera, J.M. and Calvo, J., "Dynamic recrystallization mechanisms and twining evolution during hot deformation of Inconel 718." Mater. Sci. Eng. A, 2016, 678, 137-152.

[4]. Ni, M., Chen, C., Xu, R., Hosseini, S.R.E., Li, R., Zhang, X. and Zhou, K., "Microstructure and mechanical properties of additive manufactured Inconel 718 alloy strengthened by oxide dispersion with 0.3 wt% Sc addition." J. Alloys Compd., 2022, 918, 165763.

[5]. Sahu, A.K. and Bag, S., "Probe pulse conditions and solidification parameters



[ DOI: 10.22068/ijmse.3304 ]

for the dissimilar welding of Inconel 718 and AISI 316L stainless steel." Metall. Mater. Trans. A, 2020, 51, 2192-2208.

[6]. Mostafaei, A., Ghiaasiaan, R., Ho, I.T., Strayer, S., Chang, K.C., Shamsaei, N., Shao, S., Paul, S., Yeh, A.C., Tin, S. and To, A.C., "Additive Manufacturing of Nickel-based superalloys: a state-of-the-art review on process-structure-defect-property relationship." Prog. Mater. Sci., 2023, 136, 101108.

[7]. Tekoğlu, E., O'Brien, A.D., Liu, J., Wang, B., Kavak, S., Zhang, Y., Kim, S.Y., Wang, S., Ağaoğulları, D., Chen, W. and Hart, A.J., "Strengthening additively manufactured Inconel 718 through in-situ formation of nanocarbides and silicides." Addit. Manuf., 2023, 67, 103478.

[8]. Khodabakhshi, F., Hasani, N., Kalaie, M.R., Hadadzadeh, A., Wells, M.A. and Mohammadi, M., "Dynamic recrystallization under hot deformation of additively manufactured 316 L stainless steel." Mater. Charact., 2023, 202, 113055.

[9]. Kangazian, J., Shamanian, M., Kermanpur, A., Sadeghi, F. and Foroozmehr, E., "An investigation on the microstructure and compression properties of laser powder-bed fusion fabricated Hastelloy X Ni-based superalloy honeycomb structures." Mater. Sci. Eng. A, 2022, 853, 143797.

[10]. Behjat, A., Shamanian, M., Taherizadeh, A., Lannunziata, E., Bagherifard, S., Gadalińska, E., Saboori, A. and Iuliano, L., "Microstructure-electrochemical behavior relationship in post processed AISI316L stainless steel parts fabricated by laser powder bed fusion." J. Mater. Res. Technol., 2023, 23, 3294-3311.

[11]. Tabatabaei, N., Zarei-Hanzaki, A., Moshiri, A. and Abedi, H.R., "The effect of heat treatment on the room and high temperature mechanical properties of AlSi10Mg alloy fabricated by selective laser melting." J. Mater. Res. Technol., 2023, 23, 6039-6053.

[12]. Azami, M., Siahsarani, A., Hadian, A., Kazemi, Z., Rahmatabadi, D., Kashani-Bozorg, S.F. and Abrinia, K., "Laser powder bed fusion of Alumina/Fe–Ni ceramic matrix particulate composites impregnated with a polymeric resin." J. Mater. Res. Technol., 2023, 24, 3133-3144.

[13]. Ghashghay, B.R., Abedi, H.R. and Shabestari, S.G., "On the capability of grain refinement during selective laser melting of AlSi10Mg alloy." J. Mater. Res. Technol., 2023, 24, 9722-9730.

[14]. Hosseini, E. and Popovich, V.A., "A review of mechanical properties of additively manufactured Inconel 718." Addit. Manuf., 2019, 30, 100877.

[15]. Ghaemifar, S. and Mirzadeh, H., "Precipitation kinetics of niobium carbide (NbC) during homogenization heat treatment of additively manufactured Inconel 718 superalloy." J. Mater. Res. Technol., 2023, 25, 1774-1781.

[16]. Laleh, M., Sadeghi, E., Revilla, R.I., Chao, Q., Haghdadi, N., Hughes, A.E., Xu, W., De Graeve, I., Qian, M., Gibson, I. and Tan, M.Y., "Heat treatment for metal additive manufacturing." Prog. Mater. Sci., 2022, 133, 101051.

[17]. Raghavan, S., Zhang, B., Wang, P., Sun, C.N., Nai, M.L.S., Li, T. and Wei, J., "Effect of different heat treatments on the microstructure and mechanical properties in selective laser melted INCONEL 718 alloy." Mater. Manuf. Process., 2017, 32, 1588-1595.

[18]. Ghaemifar, S. and Mirzadeh, H., "Dissolution kinetics of Laves phase during homogenization heat treatment of additively manufactured Inconel 718 superalloy." J. Mater. Res. Technol., 2023, 24, 3491-3501.

[19]. Cao, M., Zhang, D., Gao, Y., Chen, R., Huang, G., Feng, Z., Poprawe, R., Schleifenbaum, J.H. and Ziegler, S., "The effect of homogenization temperature on the microstructure and high temperature mechanical performance of SLM-fabricated IN718 alloy." Mater. Sci. Eng. A, 2021, 801, 140427.

[20]. Zhang, H., Li, C., Guo, Q., Ma, Z., Li, H. and Liu, Y., "Improving creep resistance of nickel-based superalloy Inconel 718 by tailoring gamma double prime variants." Scr. Mater., 2019, 164, 66-70.

[21]. Zhao, Y., Guan, K., Yang, Z., Hu, Z., Qian, Z., Wang, H. and Ma, Z., "The effect of subsequent heat treatment on the evolution



[ DOI: 10.22068/ijmse.3304 ]

behavior of second phase particles and mechanical properties of the Inconel 718 superalloy manufactured by selective laser melting." Mater. Sci. Eng. A, 2020, 794, 139931.

[22]. Rafiei, M., Mirzadeh, H. and Malekan, M., "Delta processing effects on the creep behavior of a typical Nb-bearing nickel-based superalloy." Vacuum, 2021, 184, 109913.

[23]. Sohrabi, M.J. and Mirzadeh, H., "Unexpected formation of delta (δ) phase in as-cast niobium-bearing superalloy at solution annealing temperatures." Materials Letters, 2020, 261, 127008.

[24]. Rafiei, M., Mirzadeh, H., Malekan, M. and Sohrabi, M.J., "Homogenization kinetics of a typical nickel-based superalloy." J. Alloys Compd., 2019, 793, 277-282.

[25]. Rafiei, M., Mirzadeh, H. and Malekan, M., "Precipitation kinetics of γ″ phase and its mechanism in a Nb-bearing nickel-based superalloy during aging." Vacuum, 2020, 178, 109456.

[26]. Huang, W., Yang, J., Yang, H., Jing, G., Wang, Z. and Zeng, X., "Heat treatment of Inconel 718 produced by selective laser melting: Microstructure and mechanical properties." Mater. Sci. Eng. A, 2019, 750, 98-107.

[27]. Ghaemifar, S. and Mirzadeh, H., "Precipitation kinetics of gamma double prime phase during direct aging treatment of Inconel 718 superalloy additively manufactured by selective laser melting." J. Mater. Res. Technol., 2023, 27, 4248-4255.

[28]. Popovich, V.A., Borisov, E.V., Popovich, A.A., Sufiiarov, V.S., Masaylo, D.V. and Alzina, L., "Impact of heat treatment on mechanical behaviour of Inconel 718 processed with tailored microstructure by selective laser melting." Mater. Des., 2017, 131, 12-22.

[29]. Wang, X., Gong, X. and Chou, K., "Review on powder-bed laser additive manufacturing of Inconel 718 parts." Proc. Inst. Mech. Eng., Part B, 2017, 231, 1890-1903.

[30]. Chlebus, E., Gruber, K., Kuźnicka, B., Kurzac, J. and Kurzynowski, T., "Effect of heat treatment on the microstructure and mechanical properties of Inconel 718 processed by selective laser melting." Mater. Sci. Eng. A, 2015, 639, 647-655.

[31]. Sohrabi, M.J. and Mirzadeh, H., "Numerical and analytical solutions for determination of interdiffusion coefficients in superalloys during homogenization." Mater. Today Commun., 2019, 21, 100631.

[32]. Sohrabi, M.J. and Mirzadeh, H., "Estimation of homogenisation time for superalloys based on a new diffusional model." Mater. Sci. Technol., 2020, 36, 380-384.

[33]. Shajari, Y., Seyedraoufi, Z.S., Alizadeh, A., Razavi, S.H., Porhonar, M. and Mirzavand, K., "Effect of solution temperature of rejuvenation heat treatment on the stability of γ′ precipitates in Ni-base superalloy IN738LC during long-term heating." Mater. Res. Express, 2019, 6, 126571.

[34]. Razavi, S.H., Mirdamadi, S.H., Szpunar, J. and Arabi, H., "Improvement of age-hardening process of a nickel-base superalloy, IN738LC, by induction aging." J. Mater. Sci., 2002, 37, 1461-1471.

[35]. Yu, X., Lin, X., Liu, F., Wang, L., Tang, Y., Li, J., Zhang, S. and Huang, W., "Influence of post-heat-treatment on the microstructure and fracture toughness properties of Inconel 718 fabricated with laser directed energy deposition additive manufacturing." Mater. Sci. Eng. A, 2020, 798, 140092.

[36]. Zhang, H., Gu, D., Ma, C., Guo, M., Yang, J. and Wang, R., "Effect of post heat treatment on microstructure and mechanical properties of Ni-based composites by selective laser melting." Mater. Sci. Eng. A, 2019, 765, 138294.

[37]. Zhao, Y., Li, K., Gargani, M. and Xiong, W., "A comparative analysis of Inconel 718 made by additive manufacturing and suction casting: Microstructure evolution in homogenization." Addit. Manuf., 2020, 36, 101404.

[38]. Bertsch, K.M., De Bellefon, G.M., Kuehl, B. and Thoma, D.J., "Origin of dislocation structures in an additively manufactured austenitic stainless steel 316L." Acta Mater., 2020, 199, 19-33.

[39]. Wang, P., Qi, J.F., Chen, Z.W., Lao, C.S.,



[ DOI: 10.22068/ijmse.3304 ]

He, T.B., Lu, T.W., Gargarella, P. and Scudino, S., "Microstructure and mechanical properties of novel high-entropy alloy particle reinforced aluminum matrix composites fabricated by selective laser melting." J. Alloys Compd., 2021, 868, 159197.

[40]. Park, J.M., Asghari-Rad, P., Zargaran, A., Bae, J.W., Moon, J., Kwon, H., Choe, J., Yang, S., Yu, J.H. and Kim, H.S., "Nano-scale heterogeneity-driven metastability engineering in ferrous medium-entropy alloy induced by additive manufacturing." Acta Mater., 2021, 221, 117426.



[ DOI: 10.22068/ijmse.3304 ]